RADIATION RESEARCH 175, 282–290 (2011)
0033-7587/11 $15.00

DOI: 10.1667/RR2125.1

Adapting the γ-H2AX Assay for Automated Processing in Human Lymphocytes. 1. Technological Aspects

Helen C. Turner,[a,1] David J. Brenner,[a] Youhua Chen,[b] Antonella Bertucci,[a] Jian Zhang,[b] Hongliang Wang,[b] Oleksandra V. Lyulko,[a] Yanping Xu,[a] Igor Shuryak,[a] Julia Schaefer,[a] Nabil Simaan,[c] Gerhard Randers-Pehrson,[a] Y. Lawrence Yao,[b] Sally A. Amundson[a] and Guy Garty[a]

[a] *Center for Radiological Research, Columbia University Medical Center, New York, New York 10032;* [b] *Department of Mechanical Engineering, Columbia University, New York, New York 10027; and* [c] *Department of Mechanical Engineering, Vanderbilt University, Nashville, Tennessee 37235*

Turner, H. C., Brenner, D. J., Chen, Y., Bertucci, A., Zhang, J., Wang, H., Lyulko, O. V., Xu, Y., Shuryak, I., Schaefer, J., Simaan, N., Randers-Pehrson, G., Yao, Y. L., Amundson, S. A. and Garty, G. Adapting the γ-H2AX Assay for Automated Processing in Human Lymphocytes. 1. Technological Aspects. *Radiat. Res.* 175, 282–290 (2011).

The immunofluorescence-based detection of γ-H2AX is a reliable and sensitive method for quantitatively measuring DNA double-strand breaks (DSBs) in irradiated samples. Since H2AX phosphorylation is highly linear with radiation dose, this well-established biomarker is in current use in radiation biodosimetry. At the Center for High-Throughput Minimally Invasive Radiation Biodosimetry, we have developed a fully automated high-throughput system, the RABIT (Rapid Automated Biodosimetry Tool), that can be used to measure γ-H2AX yields from fingerstick-derived samples of blood. The RABIT workstation has been designed to fully automate the γ-H2AX immunocytochemical protocol, from the isolation of human blood lymphocytes in heparin-coated PVC capillaries to the immunolabeling of γ-H2AX protein and image acquisition to determine fluorescence yield. High throughput is achieved through the use of purpose-built robotics, lymphocyte handling in 96-well filter-bottomed plates, and high-speed imaging. The goal of the present study was to optimize and validate the performance of the RABIT system for the reproducible and quantitative detection of γ-H2AX total fluorescence in lymphocytes in a multiwell format. Validation of our biodosimetry platform was achieved by the linear detection of a dose-dependent increase in γ-H2AX fluorescence in peripheral blood samples irradiated *ex vivo* with γ rays over the range 0 to 8 Gy. This study demonstrates for the first time the optimization and use of our robotically based biodosimetry workstation to successfully quantify γ-H2AX total fluorescence in irradiated peripheral lymphocytes.

INTRODUCTION

Interest in radiation biodosimetry has increased greatly given the growing concern over possible radiological or nuclear terrorist attacks. Accurate methods for measuring the biological effects of radiation are critical for estimating the health risk from radiation exposure for many individuals. The direct measurement of radiation-induced DNA double-strand breaks (DSBs) in peripheral lymphocytes is one approach that provides a useful end point for triage. DNA DSBs are critical lesions that can promote genomic instability (*1–3*). Organisms have evolved complex signal transduction, cell cycle checkpoint and repair pathways, often with multiple redundancies, to respond to and repair DSBs (*4*). There is much evidence that links global DSB repair capacity with cancer risks (*5*), with radiation sensitivity (*6*), and with response to cancer therapy (*7*). One of the earliest known responses to DSB induction is the phosphorylation of thousands of molecules of the histone H2AX variant at the break site (*8*), initiated by the activation of one or more of the P13K-like kinases, a family including ataxia telangiectasia mutated (ATM), ataxia telangiectasia and Rad3-related (ATR), and DNA-dependent protein kinase (DNA-PK), as well as many other DNA repair and checkpoint proteins (*2, 9*).

Immunofluorescence microscopy has shown that phosphorylated H2AX (γ-H2AX) forms visible, discrete nuclear γ-H2AX foci at DNA DSB sites after exposure to ionizing radiation (*10, 11*). The number of γ-H2AX foci has been shown to closely correspond to the number of DSBs, with each DSB yielding one focus (*12*). Further studies showed that the formation of γ-H2AX foci at the DNA damage site is fast, with γ-H2AX foci forming within 3–15 min and reaching their maximum within 30 min of irradiation (*1, 13–15*) and subsequently dephosphorylating over the next few hours (*15–17*). Recent studies have shown that some foci may remain up to 48 h or longer (*18*). The yield of γ-H2AX has been shown to be linearly related to radiation dose, both when counting foci (*19*) and when quantifying total γ-H2AX yield by gel analysis (*8*) or fluorescence labeling (*20–22*). The efficiency of γ-H2AX detection as a biomarker for DNA DSBs makes this protein a good

[1] Address for correspondence: Center for Radiological Research, Columbia University Medical Center, 630 West 168th St., New York, NY 10032; e-mail: ht2231@columbia.edu.

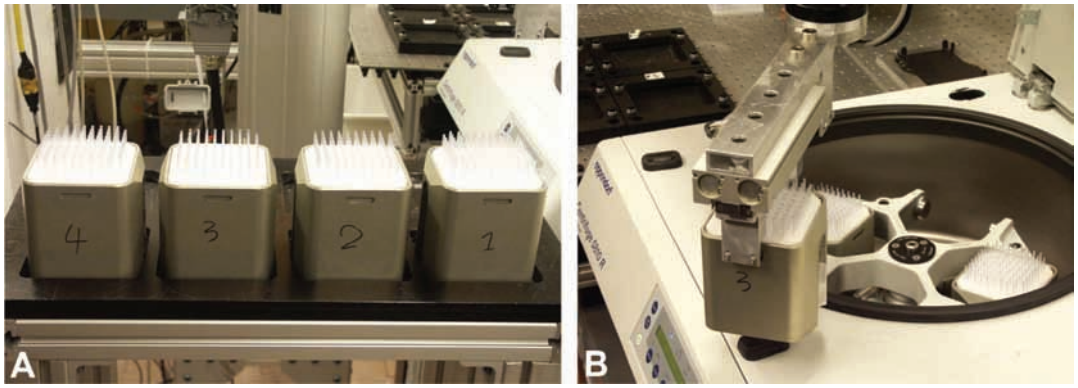

FIG. 1. RABIT input stage. Four centrifuge buckets each holding 96 capillaries are manually loaded into the input stage of the RABIT workstation (panel A); the SCARA robot automates the transfer of each bucket in the centrifuge (panel B).

candidate as a therapeutic marker for improving the efficiency of radiation, drug and other therapies (*23*).

At the Center for High-Throughput Minimally Invasive Radiation Biodosimetry, we have developed a Rapid Automated Biodosimetry Tool (RABIT) that has been designed as a completely automated, robotically based biodosimetry workstation for use after a small- or large-scale radiological event to quickly determine individual dose estimates from fingerstick-derived samples of blood (*24–27*). The workstation consists of the following modules: sample collection, lymphocyte isolation, liquid/plate handling, image acquisition and processing and data storage, with the purpose that once the blood samples are loaded into the RABIT system, there is no further human intervention. To achieve high throughput, the main technical innovations of the RABIT system over manual processing are (1) the use of smaller samples, i.e. a single 30-μl drop of blood from a fingerstick, (2) complete automation of the biology protocol, with *in situ* imaging in filter-bottomed multiwell plates, and (3) innovations in high-speed imaging. Rather than counting foci, which requires high-resolution 3D imaging (*28–30*) and underestimates doses above about 2 Gy due to focus overlap (*22, 28*), we have chosen a simpler, faster and more reliable (at high doses) approach of measuring the total fluorescence per nucleus of immunostained γ-H2AX. The advantage of this approach is that it allows a rapid quantitative result even at high doses, where individual foci cannot be readily distinguished.

In the present study, we describe the optimization of the RABIT's automated modules for reproducibly isolating lymphocytes from small volumes (<30 μl) of whole blood in heparin-coated PVC capillaries, subsequently releasing them into the multiwell plates and immunolabeling them to obtain γ-H2AX yields *in situ* using our robotic liquid handling system. At the time of writing, the automated imaging system is not fully optimized; its testing will be described in detail in a future paper. To adapt the γ-H2AX assay protocol for the RABIT, the cell harvesting and liquid handling components of the RABIT were optimized to reproducibly produce lymphocytes of normal rounded size and shape in each of the microwells. To evaluate the overall performance of the RABIT, γ-H2AX total fluorescence measurements were determined in lymphocyte nuclei from blood samples collected from four healthy female volunteers aged 40–50 years, irradiated (*ex vivo*) with a range of γ-ray doses between 0 and 8 Gy. Statistical analysis of the γ-H2AX fluorescence data identified a linear increase in γ-H2AX expression with increasing radiation dose up to 8 Gy. The potential use of the RABIT system in large-scale studies is also discussed.

METHODS

The RABIT workstation is comprised of four automated modules: (1) lymphocyte isolation, (2) cell harvesting, (3) liquid/plate handling, and (4) image acquisition and processing. A service robot (RS80 SCARA, Stäubli Robotics, Santa Rosa, CA) transports samples between the various modules. A full description of the RABIT breadboard design and setup is given elsewhere (*25–27*).

Sample Preparation

Peripheral whole blood (2 ml) was collected from four healthy female volunteers in the age range 40 to 50 years after informed consent was obtained. For each donor, blood samples (10–30 μl) were pipetted into heparin-coated PVC capillaries (Safe-T-Fill capillaries; RAM Scientific Inc., Yonkers, NY) containing 50 μl lymphocyte separation medium (Histopaque-1083; Invitrogen, Eugene, OR) and sealed using Hemato-Seal™ tube sealing compound (Fisher Scientific, Pittsburgh, PA). We have developed a sample collection kit that allows a minimally trained sample collector to perform this in the field (*27*). The capillaries were irradiated with γ rays (0, 1, 2, 4, 6 and 8 Gy) using a Gammacell 40 ^{137}Cs irradiator (Atomic Energy of Canada, Ltd.). For each donor, a total of 96 blood-filled capillaries were prepared, 16 for each radiation dose. After irradiation, the samples were incubated at 37°C for 30 min to allow for the formation of γ-H2AX foci at the DSB sites. At the input stage of the RABIT workstation, the 96 irradiated blood samples were distributed between three 32-capillary inserts and manually loaded into a centrifuge bucket insert. Figure 1 shows the SCARA robot ready to automate the loading of four centrifuge buckets each containing 96 capillaries (Fig. 1A) into the centrifuge (Fig. 1B).

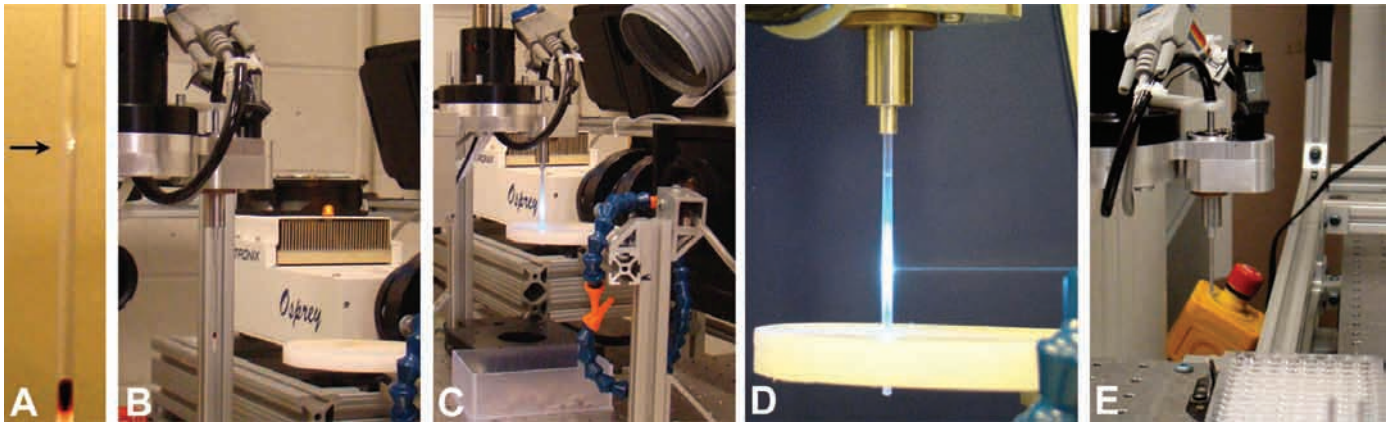

FIG. 2. Cell harvesting module. After centrifugation, the gripper arm of the SCARA robot positions the capillary tube containing the separated blood cells (panel A; arrow marks the location of the isolated lymphocyte band) in front of the UV laser (panels B, C). The laser cuts the capillary tube between the isolated lymphocyte band and RBC pellet (panel D), and the upper part of the capillary tube containing the lymphocyte band is pressure released into the microwell (panel E).

Cell Harvesting and Liquid Handling of Isolated Human Lymphocytes in the RABIT

To isolate the lymphocytes, the blood samples were spun at 3750 rpm for 5 min to form a distinct lymphocyte band at the interface between the blood plasma and the separation medium (Fig. 2A). At the cell harvesting module, the service arm of the SCARA robot with a custom-made capillary gripper extracts each capillary in turn from the centrifuge bucket and positions it in front of a 1 W UV laser (Quantronix Lasers, Osprey-355-1-0, East Setauket, NY) that cuts the capillary tube between the lymphocyte band and red blood cell (RBC) pellet (Fig. 2B–D). Laser cutting is fast with no physical contact. Furthermore, the laser is set to cut the capillary tube >10 mm away from the lymphocyte band, thus eliminating the potential for heating of the lymphocytes.

Once the RBC end of the capillary has been discarded, the service robot transports the cut capillary and pressure releases (5 PSI; 0.1 s duration) the isolated lymphocytes and plasma into a filter-bottomed multiwell plate (HTS Solubility Filter Plates with polycarbonate filters with a pore size of 0.4 μm; Millipore, Billerica, MA) containing 70 μl phosphate-buffered saline (PBS) (Fig. 2E). The time taken to pick up the capillary, locate the cutting position, cut, release each lymphocyte sample into a microwell, and dispose of the capillary is 9.7 s. To enhance the hydrophilic property of the polycarbonate membranes, the filter plates are pretreated with 50% methanol and washed twice with PBS. Once all 96 lymphocyte samples have been released, the multiwell plate is transferred to a commercial robotic plate handling system (Sciclone ALH 3000; Caliper Life Sciences, Hopkinton, MA) for automated filtering and liquid handling. The reagent reservoirs on the deck of the Sciclone workstation are programmed to perform the specific steps required for the γ-H2AX assay. As a first step, the positive pressure unit on the gantry system seals the top surface of the plate and applies a positive pressure of 2 PSI for 1.5 s, sufficient to purge the blood plasma and separation medium through the filter plates into the waste system. After the first filtration, the cells are washed by dispensing 100 μl PBS from an 8-channel bulk dispenser that is part of the functional gantry unit. After the initial wash step, the cells are fixed with 100 μl ice-cold methanol for 10 min. During this time, the filter plate is transferred to a cold surface plate set at −20°C that is incorporated into the Sciclone deck to keep the filter plate cool during the lymphocyte fixation step.

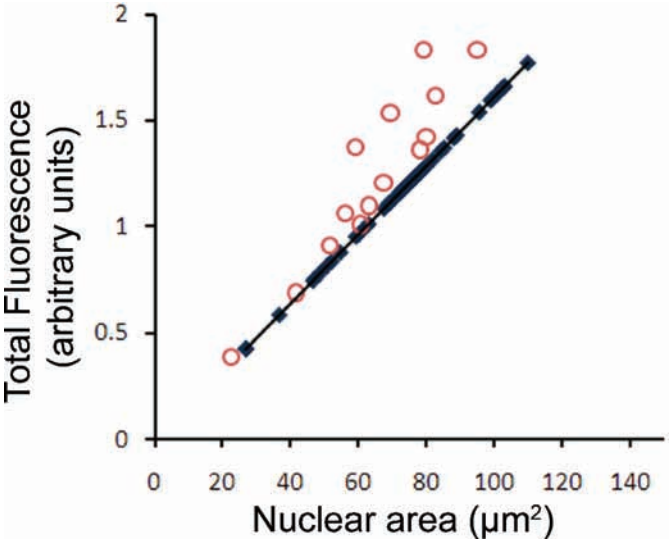

FIG. 3. Fluorescence of AF555 as a function of nuclear area at 0 and 1 Gy. The symbols correspond to fluorescence values F_i for individual unirradiated nuclei (closed symbols; values for 50 nuclei are shown) and nuclei irradiated with 1 Gy (open symbols; values for 16 nuclei are shown). For the unirradiated lymphocytes, the measured fluorescence is seen to depend linearly on nuclear area.

Immunolabeling γ-H2AX

For the immunodetection of γ-H2AX, the lymphocytes are blocked with 2% bovine serum albumin (BSA; 50 μl) for 30 min followed by exposure to an anti-human γ-H2AX monoclonal antibody (dilution 1:750; ab18311 Abcam Inc., Cambridge, MA) for 1 h at room temperature. Next, the cells are washed five times with 100 μl PBS. To visualize the γ-H2AX foci, the lymphocytes are exposed to a goat anti-mouse Alexa Fluor 555 (AF555) secondary antibody (dilution 1:1000; Invitrogen) for 50 min. The cells are then counterstained with Hoechst 33342 (2000 ng/ml; Invitrogen) for 5 min followed by a further five washes with PBS. After the final wash, the multiwell plates are moved to a transfer to substrate system (*25*) where the polycarbonate filter bottoms are detached from the multiwell plate and transferred to an adhesive surface and sealed using a transparent, low-fluorescence adhesive film (Clear View™ long lasting packaging tape; Staples, Framingham, MA). This system uses a pneumatic gripper to first remove the plate's underdrain and expose the polycarbonate membranes to adhesive rolls of film that attaches to the filters, removes and seals them. In this step, we departed from the RABIT imaging protocol, because the RABIT's

dedicated imaging system was not available for these experiments. The RABIT imaging system would load a large piece of film containing all 96 filters onto a vacuum chuck and image them sequentially, generating 12-bit grayscale images using fast (150 fps) image intensified cameras.

In this work, the sealed filter membranes were mounted manually onto microscope slides using Vectashield® mounting medium (Vector Laboratories, Burlingame, CA) and sealed with a cover slip. Images were then captured manually (250 ms integration time) with an Olympus epifluorescence microscope (Olympus BH2-RFCA; Center Valley, PA) and stored as 8-bit grayscale images using MicroSuite™ Five software (Lakewood, CO). Fluorescent images of Hoechst-labeled nuclei and AF555-labeled γ-H2AX were captured separately for each dose using a 60× oil immersion objective. The images were then analyzed using the RABIT image analysis software.

Image Analysis

Software for analysis of the paired nuclear and γ-H2AX images was written in C++, under Linux, using the Matrox Imaging Libraries (MIL 9.0, Matrox, Dorval, Canada). These libraries were chosen because they allow performing much of the image processing in hardware directly in the frame capture board of the RABIT imaging system. In brief, the image of the nuclei is filtered and binarized and the boundaries of each cell nucleus are identified using MIL's blob analysis routines. These routines identify connected regions of bright pixels within an image and can identify the size, shape, boundaries and total intensity of a grayscale image within these boundaries. For each nucleus, the integrated AF555 fluorescence intensity within each nuclear boundary is then obtained by summing the values of all pixels within the boundary (see Fig. 5):

$$F_i = \sum_{\substack{\text{Pixels within} \\ \text{nucleus } i}} \text{Pixel Value (0 } to \text{ 255).}$$

Also measured were the nuclear area A_i in pixels, the length of the perimeter, p_i, in pixels and the compactness:

$$C_i = \frac{p_i^2}{4\pi A_i}.$$

Note that a perfectly circular nucleus will have $C_i = 1$ and a more convoluted (e.g. blebbed apoptotic) one will have $C_i >> 1$. For our analysis, only nuclei with an area, A_i, larger than 20 μm^2 (3000 pixels) and a compactness of less than 2 were analyzed. For each dose 50–100 images from one well containing 40–200 nuclei were scored and the average and standard error of the mean of the fluorescence were calculated. Because the AF 555 images contain a uniform background of about 4% of the full scale (pixel values of about 10), we subtracted a background value from each nuclear fluorescence yield. The background value was obtained by fitting a graph of F_i as a function of A_i for individual unirradiated nuclei to a straight line (see Fig. 3) with slope a. The corrected fluorescence is $F_i^{corrected} = F_i - aA_i$. To avoid distortion of the measured fluorescence yields by touching nuclei that are not separated well by the software, we present here the fluorescence per pixel $f_i = F_i^{corrected}/A_i$.

RESULTS

RABIT Optimization Tests

A crucial step for the development of the γ-H2AX assay for high throughput in the RABIT was to ensure that the subsequent release of the lymphocyte cells into each microwell showed (1) adequate dispersal, (2) good cellular morphology, and (3) sufficient lymphocyte numbers to perform the assay. The first optimization tests performed in the RABIT focused on different positive filter pressures that would successfully purge the medium through the multiwell plates without affecting lymphocyte structure. To do this, we prepared a lymphocyte suspension in RPMI-1640 medium (Invitrogen) from 10–12 ml peripheral whole blood using BD Vacutainer cell preparation tubes (Becton, Dickinson and Company; Franklin Lakes, NJ). Lymphocytes were isolated according to the manufacturer's instructions. Approximately 30,000 lymphocytes were manually pipetted into each of the 96 microwells. In total, eight multiwell plates were used to test the effect of application of positive pressure values of 5, 3, 2 and 1 PSI and filtration times of 5 and 2 s. For each test, the cells were washed twice with PBS, fixed with ice-cold methanol and labeled with the nuclear stain Hoechst 33342. To visualize the Hoechst-labeled lymphocytes, the 96-well polycarbonate filter membranes were removed and sealed between the two strips of the Staples Clear View™ packaging tape and imaged using a 20× objective lens (Zeiss Axioplan 2; Carl Zeiss MicroImaging, Inc., Thornwood, NY). These preliminary tests indicated that using Sciclone positive filter pressures in the range 2 to 2.5 PSI for 2 s caused the least disruption and damage to lymphocyte nuclei and thus provided a suitable starting point for testing the liquid handling of capillary-isolated lymphocytes.

Previously, we determined that the lymphocyte band isolated from 30 μl of healthy blood samples contains ~3000 cells/μl (*27*). For the next optimization tests, lymphocytes were isolated from 10–30 μl of whole blood samples from five healthy volunteers aged 30 to 45 years. The results showed that lymphocytes isolated from 20–30 μl whole blood tended to overload the filtering capacity of the microwells as observed by unequal fluid filtration effects whereas lymphocytes isolated from 10–15 μl whole blood volumes produced an even filtration effect across all 96 wells. The remaining optimization tests sought to improve the overall integrity of cell nuclear region by further adjusting the positive filtration pressure and times and the position of the laser used to cut the capillary tubes to release the lymphocytes. Figure 4 shows the three stages of the optimization procedure. Panel A presents the results of the initial tests where the Hoechst-labeled cells were scored as unacceptable, panel B shows an intermediate step that yields suboptimal mixed quality of lymphocytes, and panel C shows cells with good, normal rounded lymphocyte integrity. We determined that laser-cutting the capillary tube too close to the lymphocyte band increased the fragility of the cells, thus causing the lymphocytes to be more susceptible to the effects of positive filtration pressure, as seen by the presence of an increased number of distorted, irregular-shaped or fragmented lymphocyte cells as seen in Fig. 4A and B.

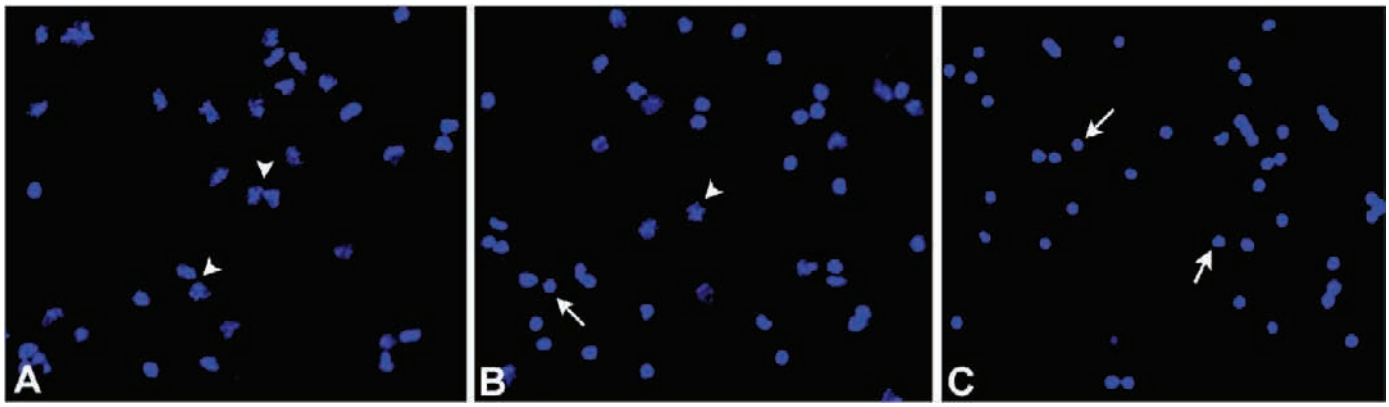

FIG. 4. RABIT optimization tests. The RABIT system was optimized for positive filtration pressure and the position of the laser to cut the capillary tubes to release the lymphocyte band into the filter plates. The panels show representative images of the results as determined by the appearance of Hoechst-labeled nuclei observed on the multiwell plate polycarbonate membranes. The lymphocytes were classified as either unacceptable (panel A), suboptimal (panel B) or optimal quality (panel C). Arrows show lymphocytes of normal rounded size and shape and arrowheads show the presence of distorted, irregular shaped or fragmented cells. Images were captured with a 20× objective lens.

Quality Control of the RABIT's Robotics System

To assess the overall reproducibility of the RABIT's robotics system to accurately dispense lymphocytes into all 96 microwells, a further five multiwell plates were prepared with peripheral blood samples from five different healthy volunteers aged 35 to 45 years. Splash tests performed by the SCARA robot showed that 5 PSI for 0.3 s was sufficient to release the lymphocyte samples into 70 µl PBS without causing any liquid carryover or splashing between the microwells. These qualitative tests were performed by placing a piece of absorbent paper under the filter plate or on a neighboring microwell. Visualization of the Hoechst-labeled nuclei for all 96 microwells confirmed the reproducibility of the RABIT's robotics system to fill better than 99.7% of the filter plate with normal rounded lymphocytes. To confirm that the laser did not induce nuclear γ-H2AX expression, one multiwell plate was prepared where half of the plate was filled with laser-cut lymphocyte samples and the other half was filled with lymphocytes that had been manually released from the capillary tubes using scissors. The γ-H2AX assay of all these samples showed that there was no increase in total γ-H2AX fluorescence in lymphocytes released using the UV laser. This can be clearly seen in Fig. 3, which show the total fluorescence in unirradiated lymphocytes from a capillary cut using the laser. The total fluorescence is linearly proportional to nuclear area, indicating that it is only due to the uniform background stemming from the imaging system. For lymphocytes irradiated with 1 Gy, all points are above the line, showing radiation-induced γ-H2AX induction.

γ-H2AX Analysis

Immunofluorescence microscopy identified the presence of increased total γ-H2AX nuclear fluorescence in lymphocytes exposed to increasing radiation dose. Figure 5 shows representative γ-H2AX fluorescence images captured as 8-bit monochrome images at a fixed exposure time of 250 ms for 0 to 8 Gy of γ rays. For the nonirradiated samples, there was no detectable background total γ-H2AX fluorescence. At doses higher than 2 Gy, γ-H2AX foci began to merge but still produced an overall increase in total fluorescence per nucleus. For each dose, a total of 50–100 images containing 40–200 cells/nuclei were captured and the total γ-H2AX fluorescence/unit area, f_i, was scored for each nucleus. The raw data were tested to see whether they were consistent with (1) a monotonic increase with dose and (2) a linear increase with dose. To determine whether the data were consistent with a monotonic increase with increasing dose, a Monte Carlo data simulation tech-

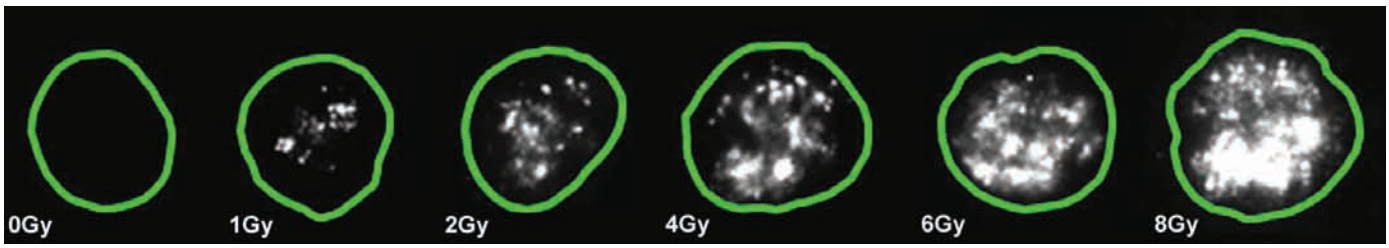

FIG. 5. γ-H2AX expression in human lymphocytes. Representative γ-H2AX staining in isolated lymphocytes irradiated with 0 to 8 Gy, visualized with Alexa Fluor 555 for cells fixed at 30 min postirradiation. The green outlines denote the boundaries of the nuclei.

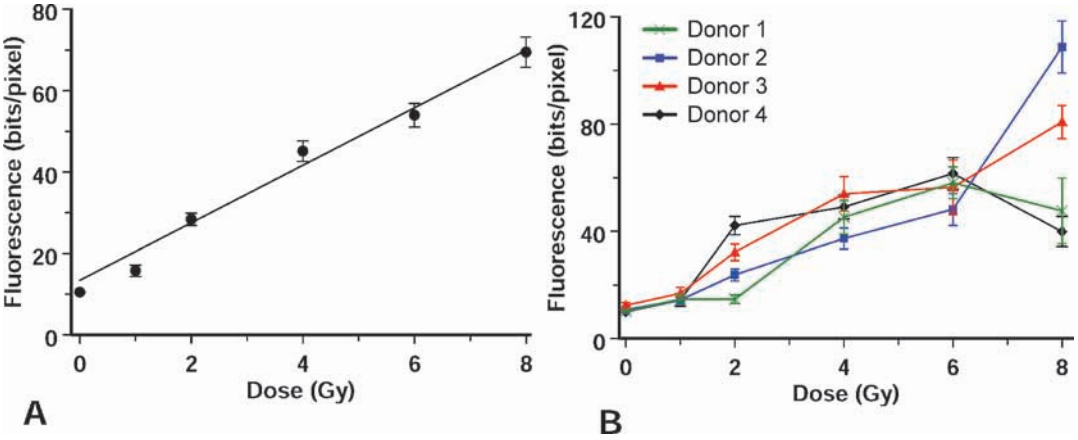

FIG. 6. Dose response for γ-H2AX analyzed 30 min after irradiation. Panel A shows a plot of the average total γ-H2AX fluorescence for the four healthy donors. Curve-fitting analysis showed that the induction of total γ-H2AX fluorescence was linear with increasing γ-ray dose up to 8 Gy. Panel B shows independent γ-H2AX fluorescence for the individual donors. Error bars are ±SEM.

nique (*31*) was used; here, based on the confidence intervals of each data point, multiple (10,000) simulated data sets were generated and each data set was checked for a monotonic increase with increasing dose. The resulting P value was 0.01, enabling us to reject the hypothesis that the data did not increase monotonically with increasing dose. To test the data for linearity, we used the standard Ramsey RESET test (*32*) in which a linear fit to the data is performed, followed by polynomial fits, with an F test used to test for significance of the nonlinear terms. Adding a quadratic term resulted in a P value of 0.23, implying that the data are adequately described by a linear model.

To test for homogeneity, linear regression analysis was performed on data from each donor individually and on pooled data from all individuals. The slopes of the individual and pooled regressions were compared by a t test. The statistical analysis showed that for doses up to and including 6 Gy the slopes for the individual donors were not significantly different from the pooled regression slope ($P > 0.05$). For doses including 8 Gy, the slopes for two of the donors, 1 and 2, were significantly different from the pooled data ($P = 0.035$ and 0.95×10^{-4}, respectively). Student's t tests confirmed that there was a significant difference ($P < 0.01$) in the total fluorescence yields at each dose up 6 Gy but not at 8 Gy. Figure 6 shows γ-H2AX dose–response curves from 0 to 8 Gy measured for 30 min postirradiation for the four healthy donors tested. The data are plotted to show the average total γ-H2AX fluorescence responses (panel A) and the individual response curves for all four donors (panel B). Errors bars show ± SEM. These results show that there is variability between the blood donors in the γ-H2AX response to ionizing radiation across all the doses, with the largest variance in the γ-H2AX total fluorescence signal seen at the highest doses of γ radiation. The two largest sources of variation in the data are (1) sensitivity of the Olympus imaging system used to manually capture the total fluorescence γ-H2AX signal and (2) intersample variation generated by capturing these images across eight microwells.

Statistical analysis of the individual data points at 2 Gy showed that there was a significant ($P < 0.01$) induction of total γ-H2AX fluorescence. Only for the data for donor 2 at 1 Gy was there no significant difference in the γ-H2AX levels 30 min postirradiation. On average more images (~200) were captured manually for 2 Gy for all four donors, which may have contributed to the improved statistical significance. The results show the largest variability in the radiation response and the greatest deviation from linearity at 8 Gy. Imaging analysis indicated an apparent increase in fragility of the cells at this dose as seen by the presence of more flattened and distorted cells. The ability of the RABIT imaging system to increase the number frames captured is likely to improve statistical analysis for the variation in the data, particularly at the lower doses. The limitation of capturing the entire dose–response curve using a fixed setting of 250 ms and an 8-bit grayscale/output is that images can potentially be underexposed at the lower doses and saturated at the higher doses. This limitation is mitigated in the RABIT imaging system currently being tested and benchmarked. The dedicated RABIT imaging system uses 12-bit, fast, intensified CMOS cameras to increase the frame capture rate, sensitivity and dynamic range. Thus, after the integration of this imaging system into the RABIT workstation, we are confident that the RABIT imaging system will accurately detect the total γ-H2AX fluorescence induced by γ rays at doses under and over 2 Gy and will accurately test the use of integrated fluorescence to quantify of γ-H2AX induction.

DISCUSSION

In previous papers (*24–27*) we described the development of the RABIT hardware with only minor consideration of biological measurements. Here we describe in detail the optimization tests performed on the RABIT system, with particular focus on the cell harvesting and liquid handling components to ensure that the prepared lymphocytes showed good cell morphology in which to perform the immunocytochemical protocol (Fig. 4). Qualitative splash tests highlighted the ability of the SCARA robot to reliably dispense lymphocytes into each of the 96 microwells. The overall goal of this study was to test the utility of our system, using the γ-H2AX assay with irradiated blood samples to establish a dose–response curve with total γ-H2AX measurements captured at 30 min postirradiation.

Central to the development of the γ-H2AX assay for automated processing in the RABIT is the use of filter-bottomed multiwell plates for high-throughput liquid handling and *in situ* imaging. The use of filter-bottomed multiwell plates also allows for rapid reagent changes and prevention of cell loss during processing. The immunostaining protocols adapted for 96-well plates in our automated system are only slight modifications of the standard manual protocols already established for the immunodetection of γ-H2AX foci using specific antibodies (*10*). To evaluate the performance of our RABIT system for the automation of the γ-H2AX immunolabeling protocol and *in situ* analysis in multiwell plates, dose–response curves were prepared from blood samples from four female healthy donors aged 40–50 years irradiated *ex vivo* with 0 to 8 Gy γ rays. Quantitative imaging of H2AX phosphorylation 30 min after exposure shows that there is an overall increase in total γ-H2AX nuclear fluorescence with increasing γ-ray dose (Fig. 5). Statistical analyses showed that the increase in total γ-H2AX fluorescence was linear with increasing dose up to 8 Gy. Testing for homogeneity suggested that γ-H2AX data for all four patients could be pooled for radiation doses up to 6 Gy (Fig. 6A). A Student's *t* test performed on these data at each dose confirmed that for the pooled data there was a significant ($P < 0.01$) increase in total γ-H2AX fluorescence up to 6 Gy. Individual Student's *t*-test analyses for the four individual donors showed a significant induction in γ-H2AX levels at 2 Gy, with only one donor showing no significant induction of γ-H2AX at 1 Gy. In the RABIT system, 0 to 2 Gy is below the point of triage, and thus variability between people exposed to lower doses is potentially of smaller consequence than not being able to establish exposures of 2 Gy and over.

Interindividual variability for γ-H2AX radiation-induced response is well documented (*20, 21*). We acknowledge that interindividual variability in the γ-H2AX signal in response to ionizing radiation is likely to be an important confounder in RABIT analyses in large-scale biodosimetry studies. The goal of future calibration experiments planned for the RABIT system is to establish calibration curves for various age-, gender- and smoking status-matched groups of individuals where individual sensitivity is built into the concept of radiation biodosimetry. The generation of multiple calibration curves for these different subpopulations is expected to partially compensate for interindividual variability, thus generating tighter confidence intervals that would be obtained from using individualized calibration curves. In Fig. 6A we have pooled data from the four donors of the same gender and age group to generate a baseline dose–response curve. These dose–response curves generated from the protocols developed at the early stages in the development of the automated RABIT system allow optimization that will lead to the generation of a baseline curve and statistical certainty to estimate dosimetry from a larger sample size in future demographic studies and real-life scenarios. Another potential confounder for RABIT imaging analyses is the effect of radiation-induced apoptosis in human lymphocytes (*33–35*). In the current system, while advanced apoptotic cells were rejected by the RABIT imaging analysis software, early apoptosis not seen as a gross change in lymphocyte morphology was included as part of the dose–response assessment. Given that apoptosis is induced in a dose-dependent manner at the doses used here, future RABIT evaluations aim to further examine the induction of apoptosis in irradiated peripheral blood lymphocytes in more detail.

It is well known that γ-H2AX levels change rapidly over time, particularly during the first 24 h. In the event of a large-scale radiological event, the collection of blood samples from thousands of exposed individuals may take several hours up to possibly 1–2 days to complete after the initial exposure. Over this time, the total γ-H2AX fluorescence signal would be expected to decrease rapidly, leaving only residual γ-H2AX levels by 24–48 h. While it is considered that in this situation the γ-H2AX yield would no longer be representative of the initial radiation dose received, and thus measurements of γ-H2AX levels at this time would be indicators of exposure and not necessarily a reflection of absorbed dose (*20*), recent *in vivo* studies have observed a dose response for γ-H2AX foci more than 48 h after irradiation in mouse skin (*36*) and in blood lymphocytes and hair samples from non-human primates.[2]

The RABIT has been designed to perform two assays, the γ-H2AX assay, as described in this paper, and the micronucleus assay (*27, 37–39*). Due to the rapid kinetics of γ-H2AX focus formation and slow decay, only samples arriving at the RABIT within 24–36 h of the

[2] C. E. Redon, A. J. Nakamura, A. Rahman, W. F. Blakely and W. M. Bonner, Gamma-H2AX as a biodosimeter for ionizing radiation exposure: an *in vivo* study with non-human primates. Presented at the 55th Annual Meeting of the Radiation Research Society, Savannah, GA, 2009.

event will be analyzed using the γ-H2AX assay. After this time, the RABIT will be reconfigured and all subsequent samples will be analyzed using the micronucleus assay. This approach allows the maximal number of samples to be analyzed using the faster γ-H2AX assay during the time window when this assay can be used. An ongoing aim of our work is to examine in more detail the γ-H2AX decay rates during the first 48 h postirradiation, with the dual goal of (1) generating a time-after-exposure-dependent calibration curve for the RABIT and (2) determining the optimal time for the switchover between the two assays. The RABIT system currently has a throughput of 6,000 samples per day and with further development could provide a practical, rapid and inexpensive tool for assessing global DSB repair capacity on an individual-by-individual basis after radiation or other genotoxic exposures or cancer treatments as well as determining global DSB damage repair capacity in a healthy population.

Conclusions

The direct visualization of the γ-H2AX repair foci using specific antibodies represents a sensitive and specific approach to directly quantify DNA DSB induction and repair caused by ionizing radiation. In the present study, we have successfully validated the use of our biodosimetry workstation to quantify γ-H2AX yields in lymphocytes isolated from small volumes of blood. Although the current application of the RABIT system is for the high-throughput reconstruction of individual past radiation exposures, future use of our unique high-throughput system could also pave the way for new individualized cancer therapy approaches and for large-scale molecular-epidemiological studies, with the long-term goal of predicting individual disease sensitivity.

ACKNOWLEDGMENTS

The authors would like to thank Marcelo Eduardo and Gary Johnson for the photographic images of the RABIT and Charles Geard and Adayabalam Balajee for useful discussions and suggestions. The authors would also like to thank the reviewers for their critical observations for the overall improvement of this manuscript. This work was supported by grant number U19 AI067773, the Center for High-Throughput Minimally Invasive Radiation Biodosimetry, from the National Institute of Allergy and Infectious Diseases, National Institutes of Health. The content is solely the responsibility of the authors and does not necessarily represent the official views of National Institute of Allergy and Infectious Diseases or the National Institutes of Health.

Received: December 18, 2009; accepted: October 10, 2010; published online: December 28, 2010

REFERENCES

1. O. A. Sedelnikova, D. R. Pilch, C. Redon and W. M. Bonner, Histone H2AX in DNA damage and repair. *Cancer Biol. Ther*. **2**, 233–235 (2003).
2. W. M. Bonner, C. E. Redon, J. S. Dickey, A. J. Nakamura, O. A. Sedelnikova, S. Solier and Y. Pommier, Gamma H2AX and cancer. *Nat. Rev. Cancer* **8**, 957–967 (2008).
3. P. J. McKinnon and K. W. Caldecott, DNA strand break repair and human genetic disease. *Annu. Rev. Genomics Hum. Genet*. **8**, 37–55 (2007).
4. M. O'Driscoll and P. A. Jeggo, The role of double-strand break repair – insights from human genetics. *Nat. Rev. Genet*. **7**, 45–54 (2006).
5. D. T. Bau, Y. C. Mau, S. L. Ding, P. E. Wu and C. Y. Shen, DNA double-strand break repair capacity and risk of breast cancer. *Carcinogenesis* **28**, 1726–1730 (2007).
6. C. E. Rube, S. Grudzenski, M. Kuhne, X. Dong, N. Rief, M. Lobrich and C. Rube, DNA double-strand break repair of blood lymphocytes and normal tissues analysed in a preclinical mouse model: implications for radiosensitivity testing. *Clin. Cancer Res*. **14**, 6546–6555 (2008).
7. D. A. Chistiakov, N. V. Voronova and P. A. Chistiakov, Genetic variations in DNA repair genes, radiosensitivity to cancer and susceptibility to acute tissue reactions in radiotherapy-treated cancer patients. *Acta Oncol*. **47**, 809–824 (2008).
8. E. P. Rogakou, D. R. Pilch, A. H. Orr, V. S. Ivanova and W. M. Bonner, DNA double-stranded breaks induce histone H2AX phosphorylation on serine 139. *J. Biol. Chem*. **273**, 5858–5868 (1998).
9. J. D. Friesner, B. Liu, K. Culligan and A. B. Britt, Ionizing radiation-dependent gamma-H2AX focus formation requires ataxia telangiectasia mutated and ataxia telangiectasia mutated and Rad3-related. *Mol. Biol. Cell* **16**, 2566–2576 (2005).
10. A. Nakamura, O. A. Sedelnikova, C. Redon, D. R. Pilch, N. I. Sinogeeva, R. Shroff, M. Lichten and W. M. Bonner, Techniques for gamma-H2AX detection. *Methods Enzymol*. **409**, 236–250 (2006).
11. N. Bhogal, F. Jalali and R. G. Bristow, Microscopic imaging of DNA repair foci in irradiated normal tissues. *Int. J. Radiat. Biol*. **85**, 732–746 (2009).
12. O. A. Sedelnikova, E. P. Rogakou, I. G. Panyutin and W. M. Bonner, Quantitative detection of ^{125}IdU-induced DNA double-strand breaks with gamma-H2AX antibody. *Radiat. Res*. **158**, 486–492 (2002).
13. E. P. Rogakou and K. E. Sekeri-Pataryas, Histone variants of H2A and H3 families are regulated during in vitro aging in the same manner as during differentiation. *Exp. Gerontol*. **34**, 741–754 (1999).
14. T. T. Paull, E. P. Rogakou, V. Yamazaki, C. U. Kirchgessner, M. Gellert and W. M. Bonner, A critical role for histone H2AX in recruitment of repair factors to nuclear foci after DNA damage. *Curr. Biol*. **10**, 886–895 (2000).
15. F. Antonelli, M. Belli, G. Cuttone, V. Dini, G. Esposito, G. Simone, E. Sorrentino and M. A. Tabocchini, Induction and repair of DNA double-strand breaks in human cells: dephosphorylation of histone H2AX and its inhibition by calyculin A. *Radiat. Res*. **164**, 514–517 (2005).
16. J. P. Banath, S. H. MacPhail and P. L. Olive, Radiation sensitivity, H2AX phosphorylation, and kinetics of repair of DNA strand breaks in irradiated cervical cancer cell lines. *Cancer Res*. **64**, 7144–7149 (2004).
17. P. L. Olive and J. P. Banath, Phosphorylation of histone H2AX as a measure of radiosensitivity. *Int. J. Radiat. Oncol. Biol. Phys*. **58**, 331–335 (2004).
18. C. E. Redon, J. S. Dickey, W. M. Bonner and O. A. Sedelnikova, gamma-H2AX as a biomarker of DNA damage induced by ionizing radiation in human peripheral lymphocytes and artificial skin. *Adv. Space Res*. **43**, 1171–1178 (2009).
19. K. Rothkamm, I. Kruger, L. H. Thompson and M. Lobrich, Pathways of DNA double-strand break repair during the mammalian cell cycle. *Mol. Cell. Biol*. **23**, 5706–5715 (2003).

20. A. Andrievski and R. C. Wilkins, The response of gamma-H2AX in human lymphocytes and lymphocytes subsets measured in whole blood cultures. *Int. J. Radiat. Biol*. **85**, 369–376 (2009).
21. I. H. Ismail, T. I. Wadhra and O. Hammarsten, An optimized method for detecting gamma-H2AX in blood cells reveals a significant interindividual variation in the gamma-H2AX response among humans. *Nucleic Acids Res*. **35**, e36 (2007).
22. S. H. MacPhail, J. P. Banath, T. Y. Yu, E. H. Chu, H. Lambur and P. L. Olive, Expression of phosphorylated histone H2AX in cultured cell lines following exposure to X-rays. *Int. J. Radiat. Biol*. **79**, 351–358 (2003).
23. J. S. Dickey, C. E. Redon, A. J. Nakamura, B. J. Baird, O. A. Sedelnikova and W. M. Bonner, H2AX: functional roles and potential applications. *Chromosoma* **118**, 683–692 (2009).
24. A. Salerno, A. Bhatla, O. V. Lyulko, A. Dutta, G. Garty, N. Simaan, G. R. Pehrson, Y. L. Yao, D. J. Brenner and J. Nie, Design considerations for a minimally invasive high-throughput automation system for radiation biodosimetry. In *Proceedings of the 3rd Annual IEEE Conference on Automation Science and Engineering*, pp. 846–852. IEEE, New York, 2007.
25. Y. Chen, H. Wang, G. Garty, Y. Xu, O. V. Lyulko, H. C. Turner, G. Randers-Pehrson, N. Simaan, Y. L. Yao and D. J. Brenner, Development of a robotically-based automated biodosimetry tool for high-throughput radiological triage. *Int. J. Biomechatron. Biomed. Robot*. **1**, 115–125 (2010).
26. Y. Chen, H. Wang, G. Garty, Y. Xu, O. V. Lyulko, H. C. Turner, G. Randers-Pehrson, N. Simaan, Y. L. Yao and D. J. Brenner, Design and preliminary validation of a rapid automated biosodimetry tool for high throughput radiological triage. In *Proceedings of the ASME 2009 International Design Engineering Technical Conferences & Computers and Information in Engineering Conference*, paper no. DETC2009-86425. ASME, New York, 2009.
27. G. Garty, Y. Chen, A. Salerno, H. Turner, J. Zhang, O. Lyulko, A. Bertucci, Y. Xu, H. Wang and D. J. Brenner, The RABIT: a rapid automated biodosimetry tool for radiological triage. *Health Phys*. **98**, 209–217 (2010).
28. W. Bocker and G. Iliakis, Computational methods for analysis of foci: validation for radiation-induced gamma-H2AX foci in human cells. *Radiat. Res*. **165**, 113–124 (2006).
29. Y. N. Hou, A. Lavaf, D. Huang, S. Peters, R. Huq, V. Friedrich, B. S. Rosenstein and J. Kao, Development of an automated gamma-H2AX immunocytochemistry assay. *Radiat. Res*. **171**, 360–367 (2009).
30. S. Roch-Lefèvre, T. Mandina, P. Voisin, G. Gaëtan, J. E. Mesa, M. Valente, P. Bonnesoeur, O. García, P. Voisin and L. Roy, Quantification of gamma-H2AX foci in human lymphocytes: a method for biological dosimetry after ionizing radiation exposure. *Radiat. Res*. **174**, 185–94 (2010).
31. W. H. Press, B. F. Flannery, S. A. Teukolsky and W. T. Vetterling, *Numerical Recipes: The Art of Scientific Computing*. Cambridge University Press, Cambridge, 1986.
32. J. B. Ramsey, Tests for specifications errors in classical linear least-squares regression analysis. *J. R. Stat. Soc. B Methods* **31**, 350–371 (1969).
33. D. R. Boreham, J. A. Dolling, S. R. Maves, N. Siwarungsun and R. E. J. Mitchel, Dose-rate effects for apoptosis and micronucleus formation in gamma-irradiated human lymphocytes. *Radiat. Res*. **153**, 579–586 (2000).
34. D. R. Boreham, K. L. Gale, S. R. Maves, J. A. Walker and D. P. Morrison, Radiation-induced apoptosis in human lymphocytes: potential as a biological dosimeter. *Health Phys*. **71**, 685–691 (1996).
35. T. Tanaka, D. Halicka, F. Traganos and Z. Darzynkiewicz, Cytometric analysis of DNA damage: phosphorylation of histone H2AX as a marker of DNA double-strand breaks (DSBs). *Methods Mol. Biol*. **523**, 161–168 (2009).
36. N. Bhogal, P. Kaspler, F. Jalali, O. Hyrien, R. Chen, R. P. Hill, and R. G. Bristow, Late residual gamma-H2AX foci in murine skin are dose responsive and predict radiosensitivity in vivo. *Radiat. Res*. **173**, 1–9 (2010).
37. M. Fenech, The lymphocyte cytokinesis-block micronucleus cytome assay and its application in radiation biodosimetry. *Health Phys*. **98**, 234–243 (2010).
38. M. Fenech, Cytokinesis-block micronucleus cytome assay. *Nat. Protoc*. **2**, 1084–1104 (2007).
39. J. P. McNamee, F. N. Flegal, H. B. Greene, L. Marro and R. C. Wilkins, Validation of the cytokinesis-block micronucleus (CBMN) assay for use as a triage biological dosimetry tool. *Radiat. Prot. Dosimetry* **135**, 232–242 (2009).